Extension and validation of an operational dynamic wake model to yawed configurations

Extension and validation of an operational dynamic wake model to yawed configurations

M Lejeune[1], **M Moens**[1], **P Chatelain**[1]

[1] Institute of Mechanics, Materials and Civil Engineering, Université catholique de Louvain, 1348 Louvain-la-Neuve, Belgium

E-mail: maxime.lejeune@uclouvain.be

Abstract. This work extends the capabilities of an operational dynamic wake model to yawed cases. The proposed framework brings together flow sensing and Lagrangian flow modeling into a unified framework: both the freestream flow field and the wake one are discretized as series of information-carrying particles. A source condition for these particles is thus obtained from the wind turbine measurements through flow sensing techniques. The estimated flow field state across the wind farm is finally reconstructed by propagating these particles downstream at their own characteristic velocity. The resulting framework is first presented and its extension to yawed turbine is then discussed. Comparison against high-fidelity Large Eddy Simulations of yawed wind turbines confirms the good potential of the approach: different yaw angles are considered and the performance of the model are evaluated. This study indicates that the proposed framework captures the relevant large scale wake features caused by the combined effect of yawing and wake meandering at a low computational cost thereby making it suitable for online model-based control.

1. Introduction

The development of new control strategies is one of the key approaches currently envisioned in order to optimize the power production and alleviate loads at the wind farm scale. Both wake redirection and induction control methodologies have been extensively explored in the literature leading to an overall improvement of the wind farm performances [1, 2].

However, due to the large convective time scales involved in wind farms, a significant delay is observed between a control input change and its impact on downstream wind turbines. Consequently, most of these studies have remained focused toward the development of model-based controllers [3]. Such controllers obviously require the use of sufficiently faithful yet computationally cheap surrogate wake models without which the synthesized control scheme may have a detrimental effect on the plant.

Literature abounds with such wake models which, for most, have been focusing on a steady-state analysis of the flow state that completely overlooks some of the key dynamic features of the wake such as meandering. They, instead, regard the wake as static and broad and assimilate wake meandering to the wake expansion as illustrated in Figure 1 [4]. This approximation works relatively well for slow wind farm control but leads to inconsistent results if finer time scales are considered. The development of operational dynamic wake tracking tools has therefore recently been gaining interest (*eg*: [5, 6]) as such models provide valuable insight for dynamic control strategies of wind turbines. These models are often based on the Dynamic Wake Meandering

model (DWM) introduced by Larsen *et al.* [7] and consider the wake as a passive tracer advected by the large scale atmospheric eddies. Other popular DWM implementations include FAST-Farm [8] which was shown to capture accurately the loads of the turbine and the associated wake dynamics [9] providing full knowledge of the inflow.

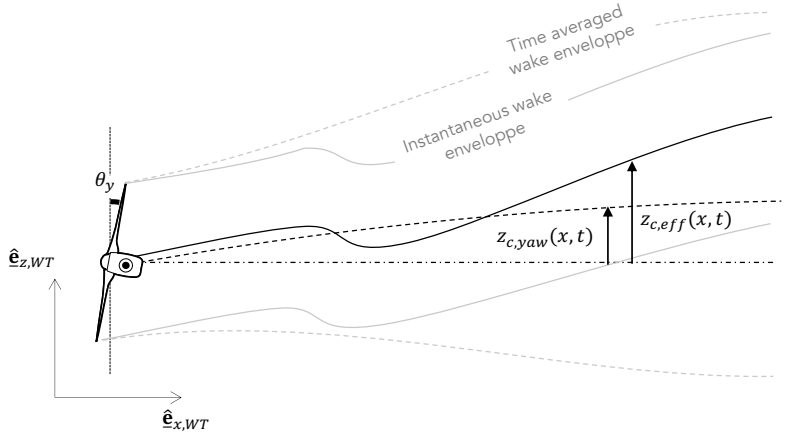

Figure 1. The static wake model assumption

The work presented here extends the capabilities of an operational dynamic wake model [10, 11] to yawed cases. The proposed framework bridges together flow sensing and wake modeling: the flow features are inferred at the wind turbine location directly from the wind turbine measurements and then advected across the wind farm thereby reconstructing the flow field. This allows to compute the impact of a control input change on the impinged rotor ahead of time as well as to anticipate the effect of the resulting wake on those rotors. A yaw module is deployed within this framework in order to capture the combined effect of wake meandering and yaw deflection. In an attempt to facilitate the online tuning procedure while keeping the resulting framework computationally tractable, focus is laid on providing a concise state description of the flow in line with the state-parameter space correction framework [12].

The resulting framework is first presented and then validated against Large Eddy Simulations (LES) of a small wind farm using advanced Actuator Disks. The statistics of wake meandering are assessed and compared against the wake model predictions and the time-averaged velocity field is studied.

2. Methodology

A yaw module is deployed within an online wake dynamic estimation tool developed as part of previous works [10, 11]. Information gathered and processed at the wind turbine location is propagated across the wind farm thereby reconstructing approximate snapshots of the flow field consistent with the observed data. This section first briefly describes the wake modeling framework used and then focuses on the yaw deflection model.

2.1. Description of the wake model

This wake modeling framework brings together flow sensing and Lagrangian flow modeling. Information is gathered at the wind turbine location and then advected across the domain at its own characteristic velocity.

The first step consists in retrieving the characteristics of the inflow and wake from the wind turbine measurements and operating settings. To that end, the inflow velocity field,

$\hat{\mathbf{u}}_{WT} = [\hat{u}_{WT}, \hat{w}_{WT}]$, is inferred from the machine response it triggers using flow sensing techniques. The wind turbines blades are thus considered as moving sensors whose flapwise and edgewise bending moments, M_f and M_e respectively, are strictly connected to the inflow streamwise velocity, $\hat{u}_{WT}$ [13, 14]. A Blade Element Momentum code fed with the flapwise bending moments is coupled with a Kalman filter in order to compute local estimates of the effective streamwise velocity over different rotor sectors. The extension of this method to the spanwise velocity component is however not trivial as this falls beyond the classical BEM theory. A Multilayer Perceptron (MLP) is thus used in order to map the wind turbine loads to the associated spanwise velocity component, $\hat{w}_{WT}$.

Once both components of the inflow velocity field have been determined, they can be used to compute an estimate of the wind turbine thrust coefficient, $\hat{C}_{T,WT}$, and inflow turbulence intensity, $\hat{TI}_{WT}$. The infered rotor state, $[\hat{\mathbf{u}}, \hat{C}_{T,WT}, \hat{TI}_{WT}]$, is then be fed to the flow model as an input.

The flow model decomposes the farm flow field, $\mathbf{u}(\mathbf{x}, t)$, into two main coupled fields: the freestream velocity field, $\mathbf{u}_f(\mathbf{x}, t)$, and the wake one, $\mathbf{\Delta u}(\mathbf{x}, t)$:

$$\mathbf{u}(\mathbf{x}, t) = \mathbf{u}_f(\mathbf{x}, t) - \mathbf{\Delta u}(\mathbf{x}, t) \tag{1}$$

As illustrated on Figure 2, the model discretizes each field as a series of information-carrying wake (W_i) and freestream (F_i) particles shed at successive time steps, t_i, and whose source condition is provided by the flow sensing data. This particle-based discretization makes the model fully-Lagrangian.

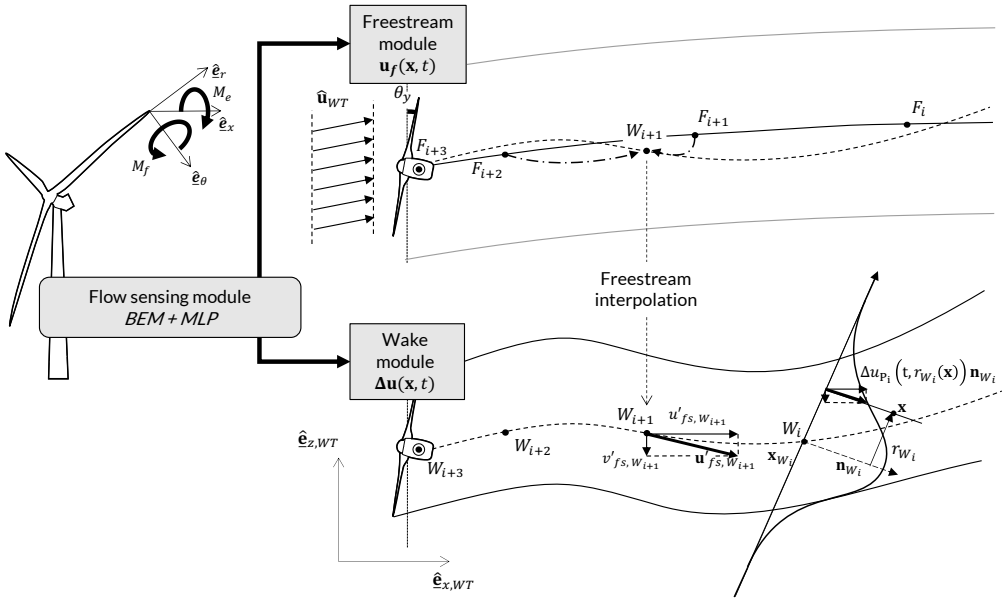

Figure 2. Description of the operational wake modeling framework proposed

Every wake particle is associated with a position, $\mathbf{x}_{W_i}(t)$, an orientation, $\mathbf{n}_{W_i}(t)$, a curvilinear coordinate along the wake centerline, ξ_{W_i}, and a speed deficit field $\Delta u_{W_i}(t, r_{W_i}(\mathbf{x}))$ where $r_{W_i}(\mathbf{x})$ and t denote the radial position of $\mathbf{x}$ relative to the wake particle and the current time respectively [8]. The particle speed deficit in the wind turbine frame, $\hat{\mathbf{e}}_{.,WT}$, is in turn obtained by projecting a simple analytic speed deficit model, Δu_{W_i} [15] along the particle orientation vector, $\mathbf{n}_{W_i}$:

$$\Delta u_{W_i}(t, r_{W_i}) = \hat{u}_{WT}(t_i) \left(1 - \sqrt{1 - \frac{\hat{C}_{T,WT}}{8(\sigma_{W_i}/D)^2}}\right) \times \exp\left(-\frac{1}{2(\sigma_{W_i}/D)^2}\left(\frac{r_{W_i}}{D}\right)^2\right) \tag{2}$$

with, D, the rotor diameter and $\sigma_{W_i}(\xi_{W_i}, \hat{C}_{T,WT})$, the effective wake width.
The wake field, $\mathbf{\Delta u}(\mathbf{x}, t)$, is then reconstructed using the passive scaler tracer assumption: the wake particles are advected downstream thereby incrementally reconstructing the wake field. In the context of isolated wakes, the convection velocity is computed from the freestream flow field, $\mathbf{u}_f(\mathbf{x}, t)$, superimposed with this self-induced speed deficit, $\Delta u_{W_i}(t, r_{W_i}(\mathbf{x}))\ \mathbf{n}_{W_i}$:

$$\tilde{\mathbf{u}}_{W_i}(t) = \mathbf{u}_f(\mathbf{x}_{W_i}, t) - \mathbf{C}_w \mathbf{\Delta u}(\mathbf{x}_{W_i}, t) \tag{3}$$

$$= \mathbf{u}_f(\mathbf{x}_{W_i}, t) - \mathbf{C}_w \Delta u_{W_i}(t, r_{W_i}(\mathbf{x}))\ \mathbf{n}_{W_i} \tag{4}$$

where $\mathbf{C}_w = [C_{w,x}, C_{w,z}]$ are tuning parameters. This expression can be generalized to multiple overlaping wakes using the standard root-sum-square weighting superposition strategy (*eg*: Jonkman *et al.* [8])

The aforementioned equation however assumes the freestream velocity field, $\mathbf{u}_f(\mathbf{x}, t)$, is known which is clearly not the case in the context of operational wake modelling. Therefore, the approach chosen here is to handle the freestream flow field in a similar fashion as the wake: the freestream flow is decomposed as a series of freestream particles, F_i, advected downstream at their own characteristic velocity, $\tilde{\mathbf{u}}_{F_i}$:

$$\tilde{\mathbf{u}}_{F_i}(t) = \mathbf{u}_f(\mathbf{x}_{F_i}, t) - \frac{C_f}{\pi R_W^2} \int_S \Delta \mathbf{u}(\mathbf{x}_{F_i}, t) \mathrm{d}s \tag{5}$$

where C_f is a tuning parameter and S denotes the circular area of radius $R_W = D$ centered at $\mathbf{x}_{F_i}$ and normal to the time-averaged freestream flow streaklines. The freestream particles are also shed from where the information is gathered: the turbine rotor where a source condition, $\mathbf{u}_{F_i}(t) = \hat{\mathbf{u}}_{WT}(t_i)$, is provided by the flow sensing module.

2.2. Yaw modeling

The characteristics of yawed wakes and most notably the deflection of their wake centerline have been extensively studied in the literature. Most these studies have adopted a pragmatic approach aimed at capturing the mean wake deflection toward wind farm control applications. The origin of the yawed wake deflection can simply be attributed to momentum conservation: the yaw offset introduces a transverse thrust force component on the wake which triggers its deflection.

In [15], Bastankhah and Porté-Agel derived a model extending the capabilities of Eq.2 to yawed wake by integrating the transverse momentum conservation equation. Another similar model is introduced by Qian *et al.* using a Gaussian speed deficit distribution along with momentum conservation [16]. Other notable efforts toward modeling yawed wake also include the higher fidelity curled wake model introduced by Martinez *et al.* which captures both wake deflection and curled shape using a vortex pair [17]. However, these efforts have been oriented toward the development of steady state models. FAST-Farm [8], on the other hand, propose to model the wake skew and deflection by orientating the speed deficit along the rotor centerline. The speed deficit is projected along the plane orientation which simultaneously allows to capture the wake deflection and skew.

This work merges together the FAST-Farm approach with some elements introduced by Bastankhah and Porté-Agel [15] in order to extend the capabilities of the wake model developed to yawed wind turbines thereby attempting to capture the combined effect of yaw and meandering wake deflection in the operational wake modeling framework.

The speed deficit equation provided by Eq.2 requires minimal adaptation as the speed deficit is expressed within the yawed plane and already accounts for the inflow skew. The particle orientation is provided by the rotor orientation at the shedding time t_i. As this model does not

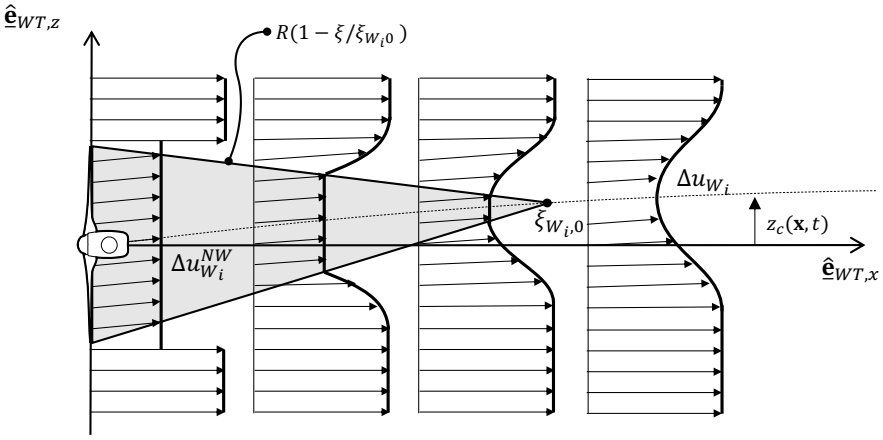

Figure 3. Idealized potential core analysis as introduced by [15]

explicitly enforce spanwise momentum conservation, particular attention should be payed toward the tuning of the $C_{w,x}$, $C_{w,z}$ and C_f parameters which govern the wake advection.

Further, in order to obtain a consistent estimate of the advection velocity, $\tilde{\mathbf{u}}_{W_i}(t)$, in the near-wake region and hence of the wake deflection, $z_c(\mathbf{x},t)$, a near-wake correction strategy should be considered. This issue is addressed by different authors who introduced new speed deficit parametrizations for the near-wake [18, 19]. However, for most, these approaches introduce new sets of tuning parameters. The idealized potential core analysis suggested by Bastankhah and Porté-Agel [15] and illustrated on Figure 3 is thus applied in order to estimate the wake convection velocity within this wake zone. Indeed, consistent with the framework presented here, their approach provides coherent estimates of the wake velocity while requiring minimal additional tuning even though it mostly overlooks the near-wake physics. The expression of the speed deficit in the near-wake zone becomes:

$$\Delta u_{W_i}^{NW}\left(t, r_{W_i}(\mathbf{x})\right) = \hat{u}_{WT}(t_i)\left(1-\sqrt{1-\hat{C}_{T,WT}}\right) \quad \text{for} \quad \frac{2r_{W_i}(\mathbf{x},t)}{D} < 1-\frac{\xi_{W_i}}{\xi_{W_i,0}}. \tag{6}$$

$\xi_{W_i,0}$ determines the end of the so-called potential core reached at the downstream location where the estimate computed using the two different speed deficit expressions collapse to the same value.

The final step consists in extending the flow sensing module to yawed rotors. This is straightforward for the streamwise velocity flow sensing as BEM methods can easily account for the aerodynamics of yawed rotors. The generalization of the transverse velocity MLP regressor to the yawed rotors, on the other hand, is still under investigation as it currently fails to capture the yaw load responses based on the current neural net inputs and associated hyperparameters set. In the current version, the transverse flow sensing module is thus disabled for yawed machines where the spanwise velocity is directly retrieved from the rotor-averaged flow field extracted from the high fidelity numerical simulation.

2.3. Model discussion

The resulting framework can, to some extent, be described as a flow sensing-based hybrid approach between the FAST-farm implementation [8] and the standard, steady-state Gaussian speed deficit introduced by [15]. Its wake-particle formulation is also analogous to the FLORIDyn observations-points approach proposed by Becker *et al.* [20].

A total number of 10 tuning parameters are introduced [11]. They govern the wake expansion (2), the wake and freestream particles advection (3 - $C_{w,x}$, $C_{w,z}$ and C_f) and finally the filter sizes used for the wake and freestream particles interpolation (5).

3. Reference simulation

The wake model predictions are compared against data recovered from high fidelity numerical simulations of a small 8 turbines farm. These turbines are distributed into two rows of 4 evenly spaced ($8D$) machines scattered inside a neutral Atmospheric Boundary Layer (ABL) as illustrated on Figure 4. The latter is characterized by a $u_h = 8\text{ms}^{-1}$ hub height streamwise velocity component associated to a moderate turbulence intensity, $TI_h = 6\%$. The simulations are performed using an in-house fourth-order finite difference LES flow solver while the turbines are based on the NREL5MW reference implemented with its torque and collective blade pitch controllers [21] and modeled using advanced actuator disks [22]. The wind turbine operates in Zone II [21], accordingly, a torque controller corresponding to a maximization of power production is applied.

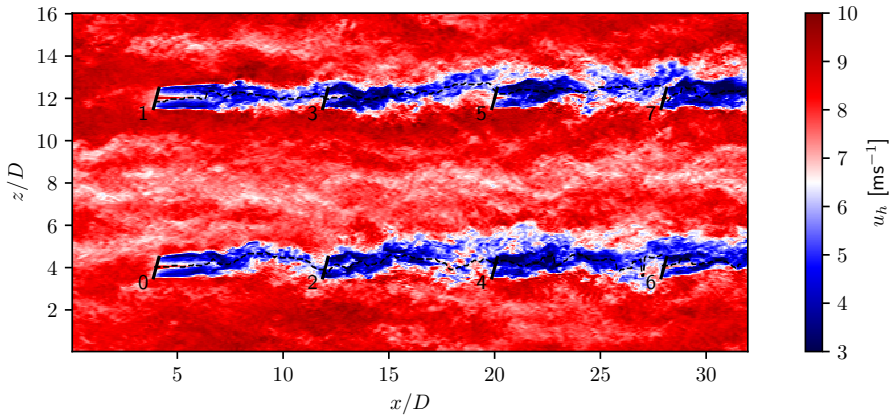

Figure 4. Streamwise velocity field measured at hub height extracted from the LES at t =1100s ($\theta_y = +15°$); position of the wake center as computed by the wake tracking algorithm (dashed black line)

The global dimensions of the simulation domain are $32D \times 8D \times 16D$ and it is discretized using resolutions of 16 and 32 points per diameter in the lateral and vertical directions respectively, which results in a grid spacing of $\Delta x = \Delta z = 7.875m$ and $\Delta y = 3.975m$. The spanwise direction is set to periodic and a rough wall law is applied on the bottom surface while a no-through flow condition is enforced at the top boundary. Finally, a concurrent precursor simulation is used guarantee the desired inflow conditions.

A wake tracking algorithm developed by Coudou [23] is applied to the LES results in order to compute the reference wake centerline (plotted in dashed black line on Figure 4) used as part of the model performance assessment. This algorithm tracks the wake centroid by seeking the position that minimizes a convolution product between the available power density in the flow and a 3D Gaussian masking function.

The simulations are run for a total of 1200s over which the yaw angle is progressively increased from 0° to 15° by steps of 5° every 300s. All of zero (ref), positive ($\theta_y > 0$) and negative ($\theta_y < 0$) yaw angles are considered and the same ABL precursor is used across all three simulations. The black lines plotted on Figure 5 show the evolution of the time averaged wake centerline positions z_c/D downstream of WT1 as a function of the normalized downstream distance, x/D. At

every steps, the wake centerline is averaged over the last 10 convective times, $T_c = u_h/D$, of each yaw step. Even though this time window considered is quite large, a strong impact of wake meandering is still present. The significant wake centerline deflection observed in the 0° reference case highlights this observation thereby further motivating the need to model both yaw and meandering induced wake deflections. The contribution of yawing to the total wake deflection can be isolated by subtracting the 0° reference case deflection from the yawed results ($\theta_y > 0$ and $\theta_y < 0$) in which case the amplitude of the yaw induced deflection roughly collapse to the same curve as illustrated on Figure 6.

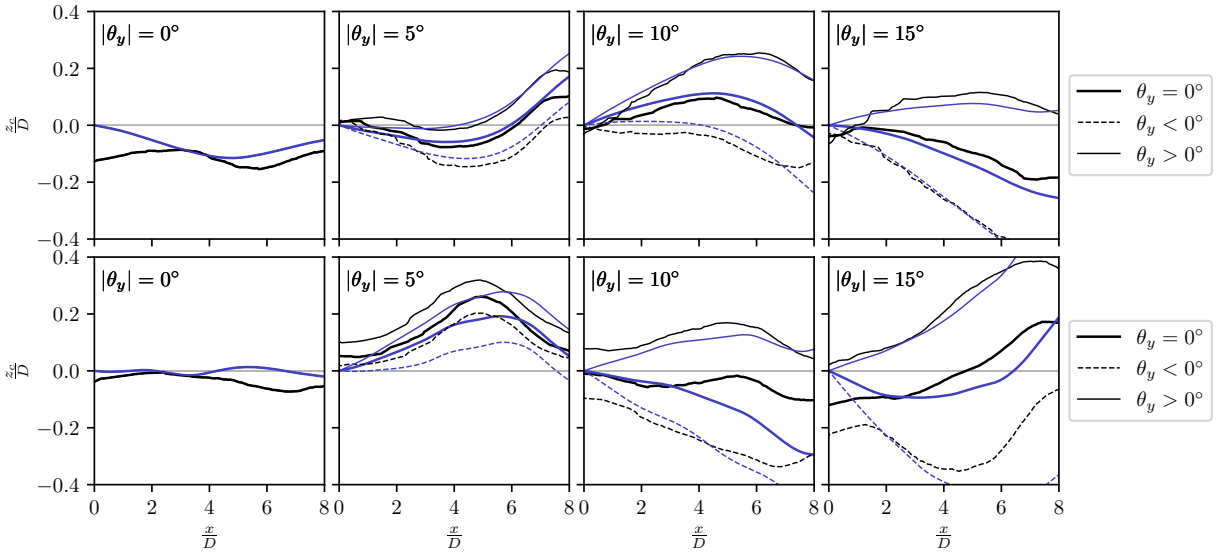

Figure 5. Normalized time averaged wake centerline z_c/D behind WT1 (top) and WT3 (bottom), averaged over the last 10 convective times of each of the yaw angle step and plotted as a function of the normalized downstream distance, x/D; LES data (black line) and wake model (blue line)

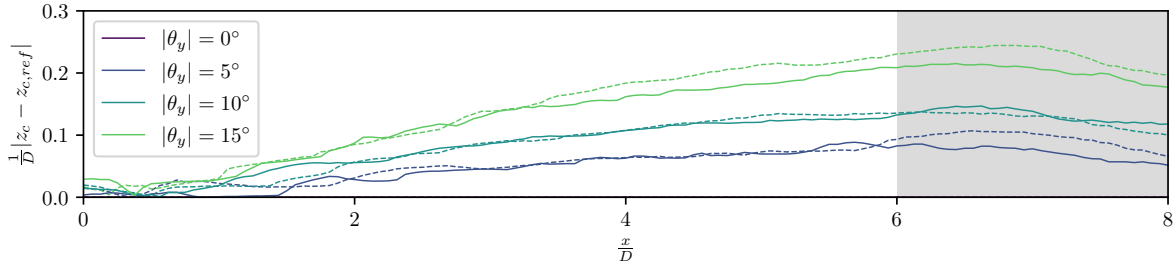

Figure 6. Amplitude of the yaw induced deflection $|z_c - z_{c,ref}|/D$ downstream WT1 averaged over the last 10 convective times of each of the yaw angle step and plotted as a function of the normalized downstream distance, x/D. Dashed line for ($\theta_y < 0$) and full line for ($\theta_y > 0$). Grayed area indicates the zone influenced by the presence of the downstream rotor.

4. Wake model performances assessment

This section presents a succinct validation of the wake modelization framework developed against the high fidelity numerical tool presented here above. The model is fed with information retrieved from the LES data and run for each yaw configurations. This data is processed by the flow sensing module and then fed to the wake model. The latter runs in fast-time as the 1200s simulation

requires around 6s to be performed sequentially on a simple laptop making it suitable for online control and ensemble-based state-parameters space correction schemes [3].

Figure 7 describes the temporal evolution of the wake centerlines behind the three first machines of the upper row of the wind farm (WT1-WT3-WT5). The wake centerline dynamics are in good agreement between the wake model developed (full line) and the actual LES data (dashed line) for all three yaw configurations and even far away from the rotor ($7D$ - bottom). This confirms the good potential of the information propagation procedure introduced even though its performances appear to degrade as we consider turbines deeper into the wind farm where the wake physics become more convoluted. This observation is confirmed by Figure 5 which depicts the spatial evolution of the time-averaged wake centerlines for all 4 yaw steps. For WT1 (top), the predictions of the wake model developed indeed allows to capture the combined effect of yaw and meandering deflections and the curves follow similar trends. The wake model fails to accurately capture the correct spatial evolution of the wake centerlines for the wind turbines deeper into the array (*eg*: WT3 - bottom). This is to be expected as the physics of yawed rotor is more convoluted leading to unmodeled wake physics [2] and inconsistent behavior of the flow sensing tools thereby undermining the overall model performances. Further, small mismatches between the wake model centerline predictions and the wake tracking algorithm are expected as the latter tracks the local individual speed deficits while the former computes the position of the associated global minima.

The two approaches are then compared in term of their instantaneous streamwise velocity profiles which further validates the previous observations. The wake model developed demonstrates good agreement with the LES data regarding this aspect as illustrated on Figure 8. Despite its simple form, Eq.6 leads to consistent estimates of the streamwise velocity component in the near wake while Eq.2 fed with the local rotor information leads to an accurate parametrization of the far wake velocity field. Both the speed deficit strength and width are accurately captured even though the model only has access to information measured at the rotor location.

5. Conclusions

In this paper, we formulated an operational wake modelization framework allowing to simultaneously capture yaw deflection and wake meandering based on wind turbine operating settings and loads. The underlying flow model reconstructs both the freestream flow field and the wake one based on the flow state inferred at the wind turbine location using a flow sensing module. Moreover, the proposed framework is formulated in line with the state-parameters correction strategy which allows to consistently capture the main dynamic features of the wake while remaining computationally tractable. Initial comparisons against high-fidelity numerical simulations indicated good prediction capabilities of the flow field at the scale of the wind farm. This shall however be confirmed by future investigations under a wider range of operating conditions.

Topics of further work also involve the extension of the transverse flow sensing module as well as the development of a state-parameters space correction strategy based on an ensemble approach in order to better account for the unmodeled physics thereby improving the overall system robustness.

Acknowledgments

This project has received funding from the European Research Council (ERC) under the European Union's Horizon 2020 research and innovation program (grant agreement no. 725627).

The present research benefited from computational resources made available on the Tier-1 supercomputer of the Fédération Wallonie-Bruxelles, infrastructure funded by the Walloon Region under the grant agreement no. 1117545.

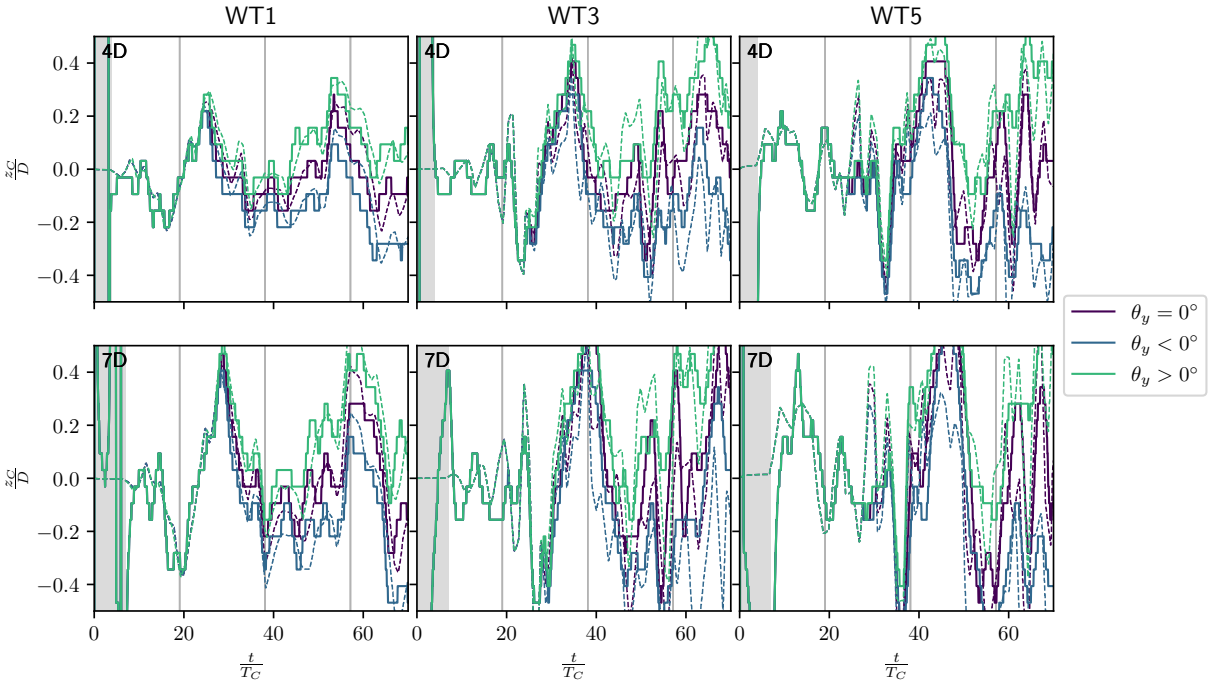

Figure 7. Temporal evolution of the instantaneous normalized wake centerline z_c/D behind WT1, WT3 and WT5 (left ro right) at two different downstream stations: $4D$ (top) and $7D$ (bottom); vertical lines indicate a step in yaw angle; grayed area indicates the startup time window

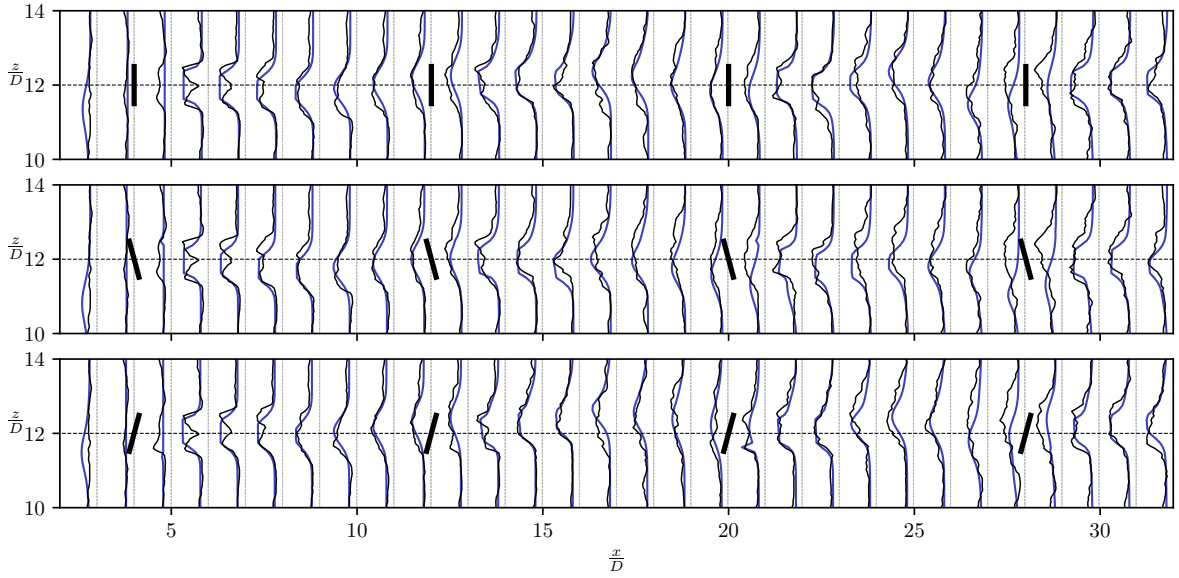

Figure 8. Comparison of the instantaneous streamwise velocity profiles at $t = 1000s$ computed by the model (blue) and by the LES data (black) for the three cases studied: $\theta_y = 0°$ (top), $\theta_y = -15°$ (middle) and $\theta_y = 15°$ (bottom)

References

[1] Larsen G, Ott S, Liew J, van der Laan M, Simon E, Thorsen G and Jacobs P 2020 *Journal of Physics: Conference Series* **1618** 062047 URL https://doi.org/10.1088%2F1742-6596%2F1618%2F6%2F062047
[2] Gebraad P M O, Teeuwisse F W, van Wingerden J W, Fleming P A, Ruben S D, Marden J R and Pao L Y 2016 *Wind Energy* **19** 95–114 (*Preprint* https://onlinelibrary.wiley.com/doi/pdf/10.1002/we.1822) URL https://onlinelibrary.wiley.com/doi/abs/10.1002/we.1822
[3] Doekemeijer B M, Van Wingerden J and Fleming P A 2019 A tutorial on the synthesis and validation of a closed-loop wind farm controller using a steady-state surrogate model *2019 American Control Conference (ACC)* (2019 American Control Conference (ACC)) pp 2825–2836 ISSN 0743-1619
[4] Thøgersen E, Tranberg B, Herp J and Greiner M 2017 *Journal of Physics: Conference Series* **854** 012017 URL https://doi.org/10.1088/1742-6596/854/1/012017
[5] Zhan L, Letizia S and Iungo G V 2020 *Wind Energy Science Discussions* **2020** 1–28 URL https://wes.copernicus.org/preprints/wes-2020-72/
[6] Lio W H, Larsen G C and Poulsen N K 2020 *Journal of Physics: Conference Series* **1618** 032036 URL https://doi.org/10.1088%2F1742-6596%2F1618%2F3%2F032036
[7] Larsen G, Madsen Aagaard H, Bingöl F, Mann J, Ott S, Sørensen J, Okulov V, Troldborg N, Nielsen N, Thomsen K, Larsen T and Mikkelsen R 2007 *Dynamic wake meandering modeling* (Risø National Laboratory) ISBN 978-87-550-3602-4
[8] Jonkman J and Shaler K 2021 Fast.farm user's guide and theory manual Tech. rep. National Renewable Energy Laboratory
[9] Jonkman J, Doubrawa P, Hamilton N, Annoni J and Fleming P 2018 *Journal of Physics: Conference Series* **1037** 062005 URL https://doi.org/10.1088%2F1742-6596%2F1037%2F6%2F062005
[10] Lejeune M, Moens M, Coquelet M, Coudou N and Chatelain P 2020 *Journal of Physics: Conference Series* **1618** 062055 URL https://doi.org/10.1088%2F1742-6596%2F1618%2F6%2F062055
[11] Lejeune M, Moens M and Chatelain P 2022 *Frontiers in Energy Research (accepted with minor revision)*
[12] Doekemeijer B M, Boersma S, Pao L Y and van Wingerden J W 2017 *2017 American Control Conference (ACC)* 19–24
[13] Bottasso C L, Cacciola S and Schreiber J 2018 *Renewable Energy* **116** 155–168 URL http://www.sciencedirect.com/science/article/pii/S0960148117309072
[14] Bertelè M and Bottasso C 2020 *Journal of Physics: Conference Series* **1618** 062022 URL https://doi.org/10.1088%2F1742-6596%2F1618%2F6%2F062022
[15] Bastankhah M and Porté-Agel F 2016 *Journal of Fluid Mechanics* 506–541
[16] Qian G W and Ishihara T 2018 *Energies* **11** ISSN 1996-1073 URL https://www.mdpi.com/1996-1073/11/3/665
[17] Martínez-Tossas L A, Annoni J, Fleming P A and Churchfield M J 2019 *Wind Energy Science* **4** 127–138 URL https://www.wind-energ-sci.net/4/127/2019/
[18] Blondel F, Cathelain M, Joulin P A and Bozonnet P 2020 *Journal of Physics: Conference Series* **1618** 062031 URL https://doi.org/10.1088%2F1742-6596%2F1618%2F6%2F062031
[19] Schreiber J, Balbaa A and Bottasso C L 2020 *Wind Energy Science* **5** 237–244 URL https://wes.copernicus.org/articles/5/237/2020/
[20] Becker M, Ritter B, Doekemeijer B, van der Hoek D, Konigorski U, Allaerts D and van Wingerden J W 2022 *Wind Energy Science Discussions* **2022** 1–25 URL https://wes.copernicus.org/preprints/wes-2021-154/
[21] Jonkman J, Butterfield S, Musial W and Scott G 2009 *National Renewable Energy Laboratory (NREL)*
[22] Moens M, Duponcheel M, Winckelmans G and Chatelain P 2018 *Wind Energy* **21** 766–782 (*Preprint* https://onlinelibrary.wiley.com/doi/pdf/10.1002/we.2192) URL https://onlinelibrary.wiley.com/doi/abs/10.1002/we.2192
[23] Coudou N, Moens M, Marichal Y, Beeck J V, Bricteux L and Chatelain P 2018 *Journal of Physics: Conference Series* **1037** 072024 URL https://doi.org/10.1088%2F1742-6596%2F1037%2F7%2F072024